Available online at www.sciencedirect.com
SCIENCE DIRECT®
Journal of Power Sources 126 (2004) 236–249
JOURNAL OF POWER SOURCES
www.elsevier.com/locate/jpowsour

# Adaptive state of charge algorithm for nickel metal hydride batteries including hysteresis phenomena

Mark Verbrugge [a,*], Edward Tate [b]

[a] General Motors Research and Development Center, Warren, MI 48090-9055, USA
[b] General Motors Powertrain Division, Troy, MI 48007-7083, USA

Received 31 July 2003; accepted 30 August 2003

**Abstract**

A state of charge (SOC) algorithm is described and implemented for a nickel metal hydride (NiMH) battery system. The essential elements of the algorithm were first used as part of the GM Precept hybrid electric vehicle program, which culminated in an 80-mile-per-gallon, 5-passenger, technology-demonstration vehicle. The algorithm is based on a simple equivalent-circuit representation of the battery pack, with the parameters adapted by means of on-line least-square regression. The output of the algorithm is the SOC, which is a measure of the available energy within the battery system, and the power capability for subsequent charge or discharge, which enables efficient hybrid vehicle operation through optimal torque allocation. The behavior of the algorithm in terms of convergence, accuracy, and robustness is examined; for these analyses, the power required from the battery for the Precept to complete a variety of drive schedules provides the power versus time trace. Voltage hysteresis is shown to play a critical role, and this effect makes determining the SOC particularly difficult for NiMH batteries relative to other battery systems (e.g., lead acid and lithium ion).


*Keywords:* Battery; Nickel metal hydride; State of charge; Algorithm; Hysteresis; Equivalent circuit; Control

## 1. Introduction

There are two terms of immediate interest to the user community of propulsion battery systems: state of charge (SOC) and state of health (SOH). The SOC corresponds to the stored charge available to do work relative to that which is available after the battery has been fully charged; this definition is made precise in the model formulation to follow. SOC can be viewed as a thermodynamic quantity, enabling one to assess the potential energy of the system. SOH is a term that is becoming more commonly used within the battery community, but which has not to date been clearly defined. Generally, SOH is used to imply that one can deduce how well the battery system is functioning relative to its nominal (rated) and end (failed) states. For our purposes, we assume that we can represent the SOH if we have a method to identify the impedance spectrum for the battery system over the frequency range of interest in an on-line (adaptive) manner. Hence, knowing the change in the SOH with time may be viewed as enabling one to assess the increase in irreversible losses that is inherent in the aging of batteries. SOH is relevant to on-board diagnostics. Thus, the system thermodynamics allow one to assess the potential energy of the system, and irreversible losses can be assessed once the impedance spectrum is known. The parameters that are used to characterize the impedance spectrum can be regressed by means of a system identification scheme. The algorithm developed in this work was applied to the Precept hybrid-electric-vehicle battery system. (See Figs. 1 and 2 for the vehicle and NiMH battery pack, respectively, [1].) The overall approach should also be useful for lead acid and lithium ion systems as well. For an analysis, overview, and summary of challenges associated with battery monitoring and energy management for electrical power systems, the paper by Meissner and Richter is quite helpful [2].

We shall determine the battery's SOC and SOH (the latter insofar as the high-frequency resistance serves a proxy for the SOH) based on least-squares recursive identification techniques. The equivalent circuit shown in Fig. 4 shall be employed to represent the essential features of the battery system. Reviews on the substantially interdependent fields of recursive identification, adaptive filters, optimal estimators, and model-reference adaptive systems (MRAS's) can be found in references [3–9]. An objective of this work

* Corresponding author. Tel.: +1-586-986-2010; fax: +1-586-986-3091.
*E-mail address:* mark.w.verbrugge@gm.com (M. Verbrugge).

0378-7753/$ – see front matter © 2003 Elsevier B.V. All rights reserved.
doi:10.1016/j.jpowsour.2003.08.042

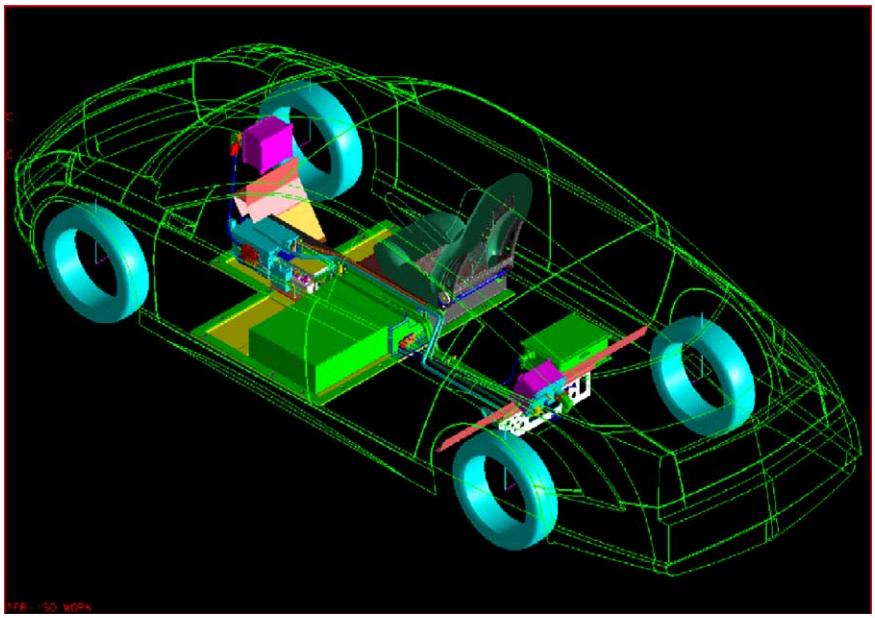

Fig. 1. Rendering of the Precept hybrid electric. The battery system is located under the front seats. The front axel has a coaxial electric traction system, and the rear axel receives torque through a traction system comprising an electric motor, a compression ignition heat engine, and a manual transmission that is automatically shifted (actuated). Regenerative braking takes place at both axels.

was to develop an equivalent-circuit model that can be used with any recursive identification scheme; the model is then combined with the least-squares method so as to regress the relevant parameters consistent with a model reference adaptive system and application in an embedded controller [7]. More complex models that include the numerical solution to coupled partial differential equations for the purposes of describing thermodynamic, kinetic, and transport phenomena from a microscopic basis [10,11] would likely lead to a prohibitively complex MRAS, as affordable embedded controllers do not have the necessary storage and execution-time capabilities today (or in the immediate future), although promising work in this area is taking place [12]. The least-squares formulation of this study amounts to

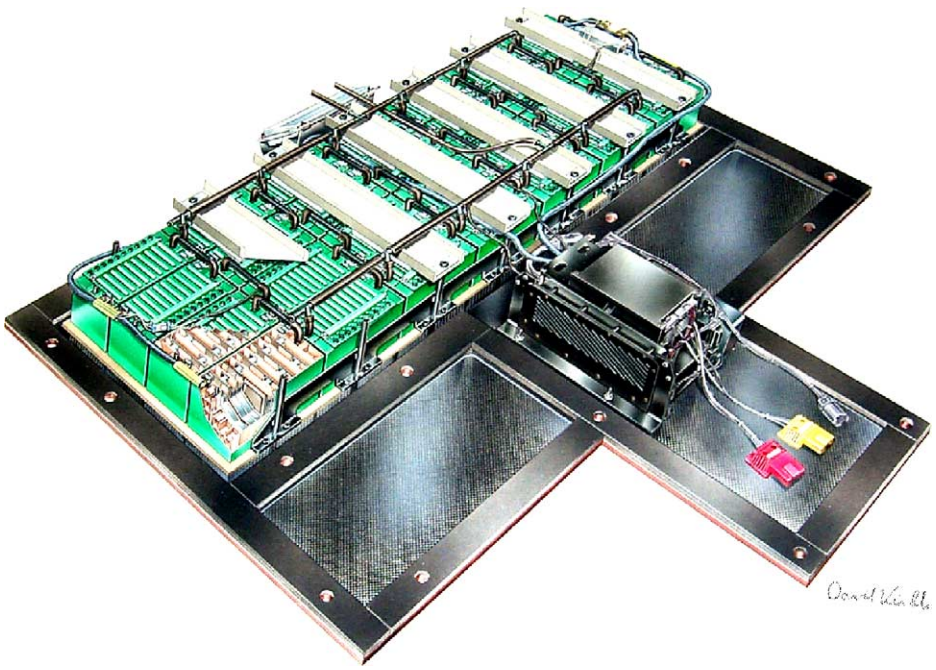

Fig. 2. Battery pack system. The 28 battery modules are liquid cooled; the coolant enters and exits at the rear of the pack. Controllers, high-voltage devices (contactors, relays, etc.) are located in front and behind the modules.

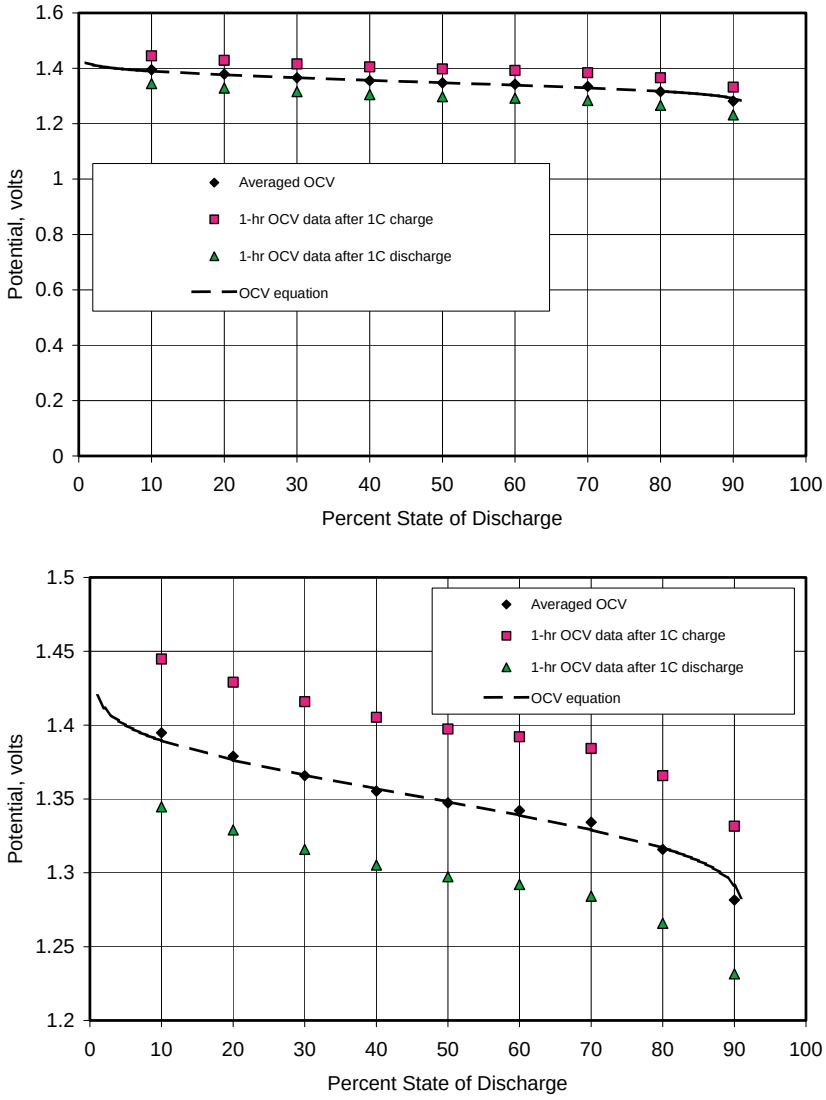


Fig. 3. Open-circuit voltages. The upper panel illustrates the flatness of the open-circuit voltage vs. SOC. The lower plot utilizes an expanded ordinate.

a fixed frame of data points, and only two parameters are regressed (the high-frequency resistance and the open-circuit voltage). As will be discussed in detail, the NiMH system is complicated by hysteresis in the open-circuit voltage (cf. Fig. 3), [13–17] which must also be regressed adaptively.

## 2. Model formulation

The model used for this estimation system consists of two parts. There is an electrical circuit model that is used to describe the relationship between the currents and voltages observed at the terminals of the battery and a coulomb-accumulation model that describes the open-circuit voltage based on the history of currents seen by the battery, including self discharge and current inefficiency on charge. The electrical circuit model is illustrated in Fig. 4. Because the SOC is a function of the open-circuit potential, extraction of the open-circuit voltage by least-squares regression leads to an estimate of the SOC. The two SOC values are referred to as $SOC_C$ (for the coulomb-accumulation

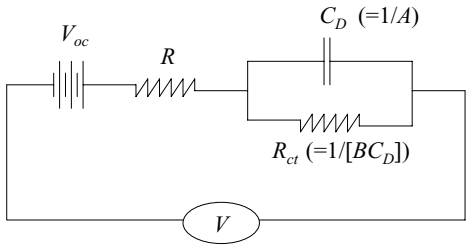


Fig. 4. Equivalent circuit for the battery system. The representation does not include self discharge, current inefficiency, temperature and SOC dependence of “circuit elements”, and hysteresis in open-circuit potential.

contribution) and $SOC_V$ (for the voltage-based contribution). Both contributions yield useful information regarding the SOC; thus a composite SOC is calculated. To find this composite SOC, the following is utilized:

$$SOC = w(SOC_C) + (1 - w)(SOC_V), \quad (1)$$

where $w$ is a weighting factor. For $SOC_C$ [18],

$$SOC_C(t) = SOC(t - \Delta t) - \int_{t-\Delta t}^{t} \left[ 100 \frac{\eta_I I}{Ah_{nominal}} + S_D(T) \right] \frac{dt}{3600}. \quad (2)$$

Time is represented by $t$, and $I$ denotes current; discharge currents are taken as positive. It is important to note that the first term on the right is SOC, not $SOC_C$; the use of the composite SOC as the first term on the right strongly couples the voltage-based and coulomb-accumulation models. For the module of this example, the nominal capacity $Ah_{nominal}$ is 12.5 Ah (35 °C, C/3 discharge rate; this quantity will have a mild temperature dependence over the range of application), and the self-discharge rate is described by [18]

$$S_D = k_0 \exp\left( -\frac{E_{A,S}}{R_g T} \right) SOC,$$

with $k_0 = 1.0683 \times 10^7$ per hour and $E_{A,S}/R_g = 6,789$ K. The current efficiency $\eta_I$ is effectively unity for the conditions near 50% SOC, as confirmed by measurements; a value of 1 is used for discharge, and 0.99 for charge; current efficiencies are expected to have a mild temperature dependence (for the conditions of this work) and decrease with increasing SOC's. The factor 3600 has units of s/h, and the factor 100 is employed to keep a consistent percent basis.

To extract the voltage-based $SOC_V$, the solution for the voltage associated with the equivalent circuit shown in Fig. 4 is employed [18–20]:

$$V = V_0 - IR + A \int_{\zeta=t}^{\zeta=0} I(\zeta) \exp[-B(t - \zeta)] \, d\zeta. \quad (3)$$

The first two terms on the right side give rise to an ohmic description of the battery, as the battery voltage $V$ is related to the open-circuit potential $V_0$ reduced by the ohmic drop $IR$, where $R$ is the battery resistance. The last term on the right side corresponds to a superposition integral, through which past currents influence the open-circuit potential beyond the first-order effect of changing the average state of charge characterizing the electrodes. (Because of the exponential weighting function, the influence of early currents is less than that of more recent currents.) An incremental improvement in the generality of the equivalent circuit would be to add a capacitor in series with the interfacial resistor $R_{ct}$ or a frequency-dependent Warburg impedance. Such additions are intended to approximate mass-transfer impedance [21–23]; the basic form of Eq. (3) does not change substantially when a capacitor is added in series with the resistor $R_{ct}$ [19]. An analysis of proton transport in nickel hydroxide can be found in the treatment by Weidner and Timmermann [24].

It is necessary to have a default value for the resistance; the approach for extracting the resistance from recorded data will be discussed below. For the NiMH battery example application in this work, the resistance data were fit to the following equation [18]:

$$R_{module} = \left( \sum_{j=1}^{n} a_j SOC^j \right) \exp\left[ -\frac{E_{A,R}}{R_g} \left( \frac{1}{T} - \frac{1}{T_{ref}} \right) \right].$$

The pack resistance is given by the number of modules multiplied by $R_{module}$ as other resistances (e.g., harnesses, etc.) have been allocated to the module resistance. (For the pack utilized in this example, 28 modules were employed. Thus, $R = N_{modules} R_{modules}$, where $N_{modules} = 28$.) The activation energy $E_{A,R}$ corresponds to $-6{,}017$ cal mol$^{-1}$. It is convenient to choose the gas constant $R_g$ with consistent units, 1.987 cal mol$^{-1}$ K$^{-1}$). The reference temperature $T_{ref}$ is chosen as 35 °C, or 308 K. The coefficients in the summation are given below. For all of the results shown in this work, the regressed resistance was subsequently bounded such that $0.5NR_{module} \le R \le 1.5NR_{module}$.

| $j$ | $a_j$ (ohms) |
|---|---|
| 0 | $4.1252 \times 10^{-2}$ |
| 1 | $8.9691 \times 10^{-4}$ |
| 2 | $1.6760 \times 10^{-5}$ |
| 3 | $-1.4435 \times 10^{-7}$ |
| 4 | $4.7223 \times 10^{-10}$ |

The open-circuit voltage (OCV) is described by a modified Nernst equation, with the inclusion of the influence of entropy of reaction and an empirical expression to capture the salient features associated with voltage hysteresis:

$$V_{oc,cell} = Function(T, SOC, V_H) = U^0 + V_H + \frac{R_g T_{ref}}{n_e F} \ln \frac{SOC - \Pi}{100 - SOC} - (\gamma)(SOC) + (T - T_{ref}) \frac{\Delta S}{n_e F} \quad (4)$$

Faraday's constant (96,487 C mol$^{-1}$) corresponds to $F$, $n_e$ denotes the electrons according to the cell reaction ($n_e = 1$ for this study), and $\Delta S$ refers to the entropy of the cell reaction, 22 J mol$^{-1}$ K$^{-1}$. (For consistent units, a value of 8.314 J mol$^{-1}$ K$^{-1}$ should be used for $R_g$ in Eq. (4).) To construct the OCV curve shown in Fig. 3, $U^0 = 1.37$ V, $\Pi = 8$ (taken as dimensionless, as is the percent state of charge), and $\gamma = 0.04$ V. The number of cells in the battery pack for this example is given by $N = 280$; thus the pack open-circuit voltage is given by $V_{oc} = NV_{oc,cell}$. The last term in Eq. (4) corresponds to a linearization of the open-circuit potential about the reference temperature, 35 °C (308 K) in this work.

For the hysteresis contribution, we construct the following first-order differential equation to formulate a cell hysteresis voltage $V_H$:

$$\frac{\partial V_H}{\partial t} = -\beta(\eta_I I - \varepsilon S_D)\left[V_{H,max} + \text{sign}(I)V_H\right]. \quad (5)$$

This equation constructs a varying hysteresis voltage; for this work, the hysteresis voltage is set up so that for prolonged charge currents, or short but very large charge currents, the hysteresis voltage tends to 50 mV per cell (for 280 cells per pack, this corresponds to 11.2 V); thus $V_{H,max} = 50$ mV per cell. The exact opposite holds for discharge (positive) currents. Note also that if the current remains at zero for a long time, the hysteresis voltage tends to the charge-decreasing condition (−50 mV per cell) through self-discharge. The ±50 mV per cell corresponds to the 100 mV per cell difference between the upper and lower open-circuit voltage curves displayed in Fig. 3; the middle curve of Fig. 3 corresponds to $V_H = 0$.

The description of the governing equations is now complete. The next section provides details regarding implementation as an SOC algorithm.

## 3. Implementation

First, the coulomb integration expression 2 is recast as:

$$\text{SOC}_C(t) = \text{SOC}(t - \Delta t) - \left[100\frac{[(\eta_I I_{t-1} + \eta_I I_t)/2]}{\text{Ah}_{\text{nominal}}} + (S_D)_{t-\Delta t}\right]\frac{\Delta t}{3600}.$$

The difference between the present time and the last recorded time is given by $\Delta t$. Next, the measured voltage expression is recast for on-line regression. First, it is helpful to note that Eq. (3) can be rewritten as the following recursion relation for evaluation purposes:

$$V|_t = (V_{oc} - IR)_t - (I|_t A)\Delta t + \exp(-B\Delta t)[V - (V_{oc} - IR)]_{t-\Delta t}, \quad (6)$$

where the subscripts $t$ and $t-\Delta t$ denote the time at which the quantities are to be evaluated. This equation is a particularly simple recursion relation in which only variables calculated at the previous time step are required to calculate the voltage at time $t$. The equation is derived in the Appendix A. To implement Eq. (6), one replaces the battery voltages with measured values:

$$\begin{aligned} V^{\text{to be used in regression}} &= \hat{V} = V^{\text{measured}}|_t + (I|_t A)\Delta t \\ &\quad - \exp(-B\Delta t)[V^{\text{measured}} - (V_{oc} - IR)]_{t-\Delta t} \\ &= (V_{oc} - IR)_t \end{aligned}$$

Thus, the regression analysis to determine the open-circuit potential and resistance is based on the voltage $\hat{V}$, the regression voltage, and a least-squares analysis of the corrected voltage data should yield a good approximation for the ohmic resistance and open-circuit potential. For all results shown in this work, $A = 0.0229\,\text{F}^{-1}$ and $B = 0.0366\,\text{s}^{-1}$ [18].

The open-circuit voltage $V_{oc}$ and the resistance $R$ are found using a least-squares approach, applied to data corresponding to a specified time interval. The following definitions are applied [25]:

$$s_I = \frac{1}{n}\sum_{j=1}^{n} I_j$$

$$s_{II} = \frac{1}{n}\sum_{j=1}^{n} I_j^2$$

$$s_V = \frac{1}{n}\sum_{j=1}^{n} \hat{V}_j$$

$$s_{IV} = \frac{1}{n}\sum_{j=1}^{n} I_j \hat{V}_j,$$

where $n$ represents the number of recorded current-potential data points to be included in the extraction of the open-circuit voltage $V_{oc}$ and the resistance $R$. For all analyses presented in this work, the time step is 1 s and $n = 91$. The summations are made effectively recursive by recognizing that a first-in, first-out method keeps the memory full of the most recent $n$ data points and does not require a full summation over all components within the sum at each time step. Using these expressions, one obtains the following,

$$R = -\frac{s_{IV} - s_I s_V}{s_{II} - (s_I)^2} \quad (7)$$

and

$$V_{oc} = \frac{s_{II} s_V - s_{IV} s_I}{s_{II} - (s_I)^2}. \quad (8)$$

These equations fail when the variance $s_{II} - s_I = 0$, or when this quantity is nearly zero. In addition, the equations can fail to provide a reasonable result when the many of the recorded currents used in the least-squares analysis are of similar value with the exception of one or two data points; thus in application it is important not to update (regress) $R$ and $V_{oc}$ when the variance is small or there is a large skewness [26] in the data.

The hysteresis contribution is now addressed. The following formulation is applied:

$$V_H(t) = w_H\{V_H - \beta(\Delta t)(\eta_I I - S_D)[V_{H,max} + \text{sign}(I)V_H]\}_{t-\Delta t} + (1 - w_H)\left[V_{oc} - U_{\text{ref}}^{\theta} - \frac{R_g T_{\text{ref}}}{n_e F}\ln\frac{\text{SOC} - \Pi}{100 - \text{SOC}} + (\gamma)\text{SOC} - (T - T_{\text{ref}})\frac{\Delta S}{nF}\right]_{t-\Delta t} \quad (9)$$

The subscript on the large brackets and braces indicates that values to the right of this equation can be evaluated at the previous time step. This equation is not a straight-forward (numerical) time integration of Eq. (5) unless the weighting factor $w_H$ is set to unity. Thus the second line of the above equation allows for a correction to the extraction of the hysteresis voltage through the recognition that the previous time step value for the SOC can be used to calculate an open-circuit voltage (cf. Eq. (4))—this back-calculated open-circuit voltage provides an adaptive routine for deducing $V_H$.

The next step is to transform the open-circuit voltage into a voltage-based state of charge, including the hysteresis voltage. To do this, the modified Nernst Eq. (4) is inverted to yield the voltage-based SOC. Rather than numerically solve a non-linear equation in an embedded controller, one can simply use a look-up table to represent the non-hysteresis portion of the modified Nernst equation.

Both the combined SOC (Eq. (1)) and the hysteresis voltage (Eq. (9)) utilize weighting factors ($w$ and $w_H$, respectively), and the influence of the time step size needs to be addressed. That is, if very small time steps are employed, then the weighting factors should be altered so that time-dependent quantities are not lost from the calculation and instead are allowed to evolve in accordance with their particular time constants. The following approach is applied in this work:

$$w = w_{\max} - \alpha_w(\Delta t) \quad \text{and} \quad w_H = w_{H,\max} - \alpha_H(\Delta t).$$

The weighting factors are bounded between 0 and 1 here. The factor $\alpha_H$ is taken as $0.005\,s^{-1}$ for all of the plots in this work. For short times (i.e., before the regression analysis allows for accurate fitting of the resistance and open-circuit potential, 91 s in this work), $w$ is set to unity, and the SOC is calculated for this short time based solely on coulomb integration from the previously stored SOC. Another special case results when the battery has been at rest for prolonged periods. In this case, the hysteresis model returns a value of $V_H$ that is less than −45 mV due to self discharge (when $\varepsilon$ is greater than zero), and the magnitude of the current is quite

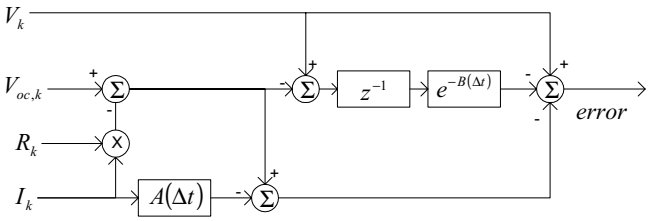


Fig. 5. Voltage-based portion of the SOC algorithm. The recursive nature of the integration is such that only quantities time steps $k$ and $k-1$ are required. The error is minimized by least-squares regression of $V_{oc}$ and $R$.

low (e.g., less than 0.1 A). In this case, the voltage-based state of charge is likely to provide the most accurate estimate for the combined SOC—an extreme case would be for a battery sitting at rest for many days, in which case the chemistry is dictated by self-discharge processes, and the charge-decreasing Nernst equation provides an accurate estimation for the battery's open-circuit potential. In such cases, $w$ can be set to a value near 0.5, which is what we have employed as a lower bound on $w$.

The quantity $\alpha_w$ is obtained as follows. First, we note that

$$\frac{\partial V_{oc}}{\partial(\mathrm{SOC})} \approx N\frac{R_g T_{ref}}{n_e F}\left[\frac{100}{\mathrm{SOC}(100-\mathrm{SOC})}\right] = \mu.$$

Thus we construct $\alpha_w$ as follows:

$$\alpha_w = \begin{cases} \text{For SOC} \geq 50\% : \alpha_w|_{50\%\mathrm{SOC}} \\ \text{For SOC} < 50\% : \min\left[10, \dfrac{\mu}{\mu|_{50\%\mathrm{SOC}}}\right] \times \alpha_w|_{50\%\mathrm{SOC}} \end{cases}$$

The quantity 10 in this equation corresponds to an upper bound used in this work, and $\alpha_w$ at 50% SOC was set to $0.001\,s^{-1}$. This approach yields larger values of $\alpha_w$ as the SOC declines below 50%, consistent with placing a greater emphasis on the voltage-base SOC when the OCV is more sensitive to changes in SOC.

A high level summary of the algorithm is depicted in Fig. 5 (for the more complicated voltage-based SOC associated with Eq. (6)) and Fig. 6 (for the entire algorithm).

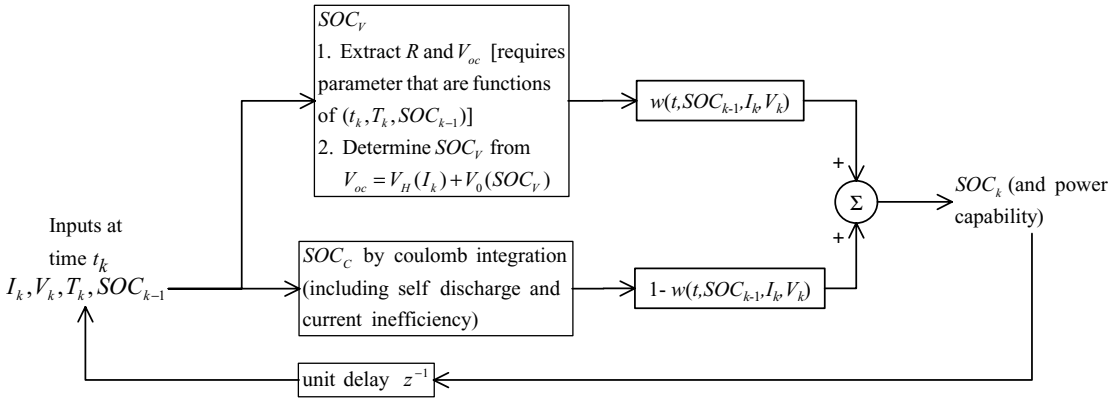


Fig. 6. Schematic overview of algorithm. The outputs are the combined SOC, the charge and discharge power capabilities. $w$ is a function of $t$, $\mathrm{SOC}_{k-1}$, $I_k$, $V_k$.

Similar schematics can be found in the controls literature for algorithm description [3–9].

## 4. Results and analysis

For all of the plots shown, the parameters values listed in Table 1 were employed unless otherwise stated. Before analyzing the specific application of the algorithm, an overview of the data shown in Fig. 7 provides a compelling reason as to why this approach is promising. A drive schedule similar to that used to determine the fuel economy values for the Precept HEV yielded the data points depicted in Fig. 7. Note that the points are substantially co-linear, and a simple ohmic-battery description ($V = V_{oc} - IR$) fit to the data captures the basic trend in the data. This result that is partially enabled by the small variation in the SOC throughout the test; if large variations in SOC are manifest, the $V_{oc}$ would not be substantially constant, and the ohmic-battery description would be less insightful. Fig. 8 can be viewed as the base case for this work, as it shows the results for the drive schedule of Fig. 7. The battery was first charged to 50% SOC, then the battery was stimulated using a power signal that approximated the operation of the battery when the vehicle is driven on the FTP driving schedule. The measured current and voltage are shown in the upper plot, along with the SOC deduced by purely coulomb counting and the open circuit voltage extracted from the data using the full algorithm. It should be stressed that we do not have a precise method to determine the error in an SOC routine, as one cannot fully discharge the batteries at low rates without damaging them. Our experience is that for the conditions of this work, the relatively short times (less than a few hours) of power cycling allows us to use the pure coulomb counting as a sufficiently accurate measure of the SOC. For longer durations (e.g., days), this would not be the case. The lower plot in Fig. 8 provides the error based on the assumption that the pure coulomb counting returns the correct answer. The percent error is taken as

Table 1
Quantities, values, and units unless otherwise specified

| Value | Units | Quantity |
|---|---|---|
| 50 | mV | Half the maximum cell hysteresis, $V_{H,max}$ |
| 12.5 | Ah | Nominal capacity at $T_{ref}$ |
| 0.0229 | $C^{-1}$ | $A$, inverse capacitance |
| 0.0366 | $s^{-1}$ | $B$, inverse time constant |
| 10 | | Cells per module ($N = 280$ cells per pack) |
| 28 | | Modules per pack |
| 0.99 | | Current efficiency at $T_{ref}$ |
| 35 | °C | Reference temperature $T_{ref}$ |
| $2.47 \times 10^{-5}$ | $C^{-1}$ | $\beta$ for charge-augmented operation |
| $3.70 \times 10^{-5}$ | $C^{-1}$ | $\beta$ for charge-depleted operation |
| 0 | Ah | $\varepsilon$, self discharge multiplier for hysteresis expression |
| 0.650 | Ω | Default high-frequency pack resistance $R$ |
| 0.001 | $s^{-1}$ | $\alpha_w$ at 50% SOC |
| 0.005 | $s^{-1}$ | $\alpha_H$ |

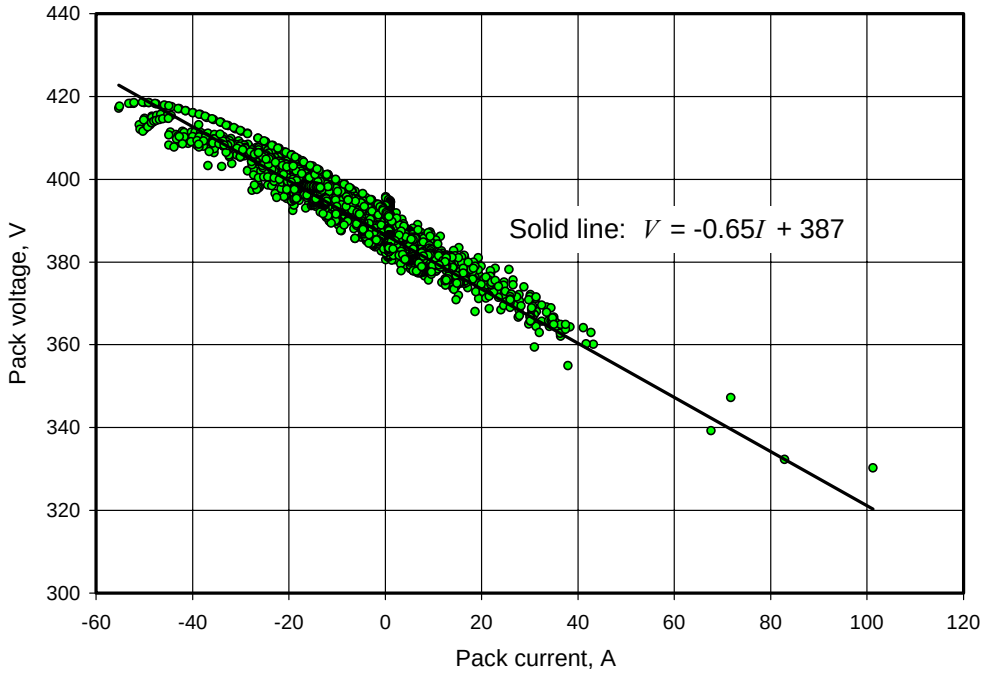


Fig. 7. Battery system current–voltage relation over a representative drive cycle. The pack power was allocated based on vehicle modeling for the Precept vehicle over a drive cycle of the following characteristics: 1384 s city schedule (FUDS), 10 min rest, 505 s of city schedule (FUDS), and two highway schedules (HWYFET). The collected current and voltage data for the described schedules correspond to the plotted data points. The fit line indicates an open-circuit voltage of 387 V, reflecting about 50% SOC.

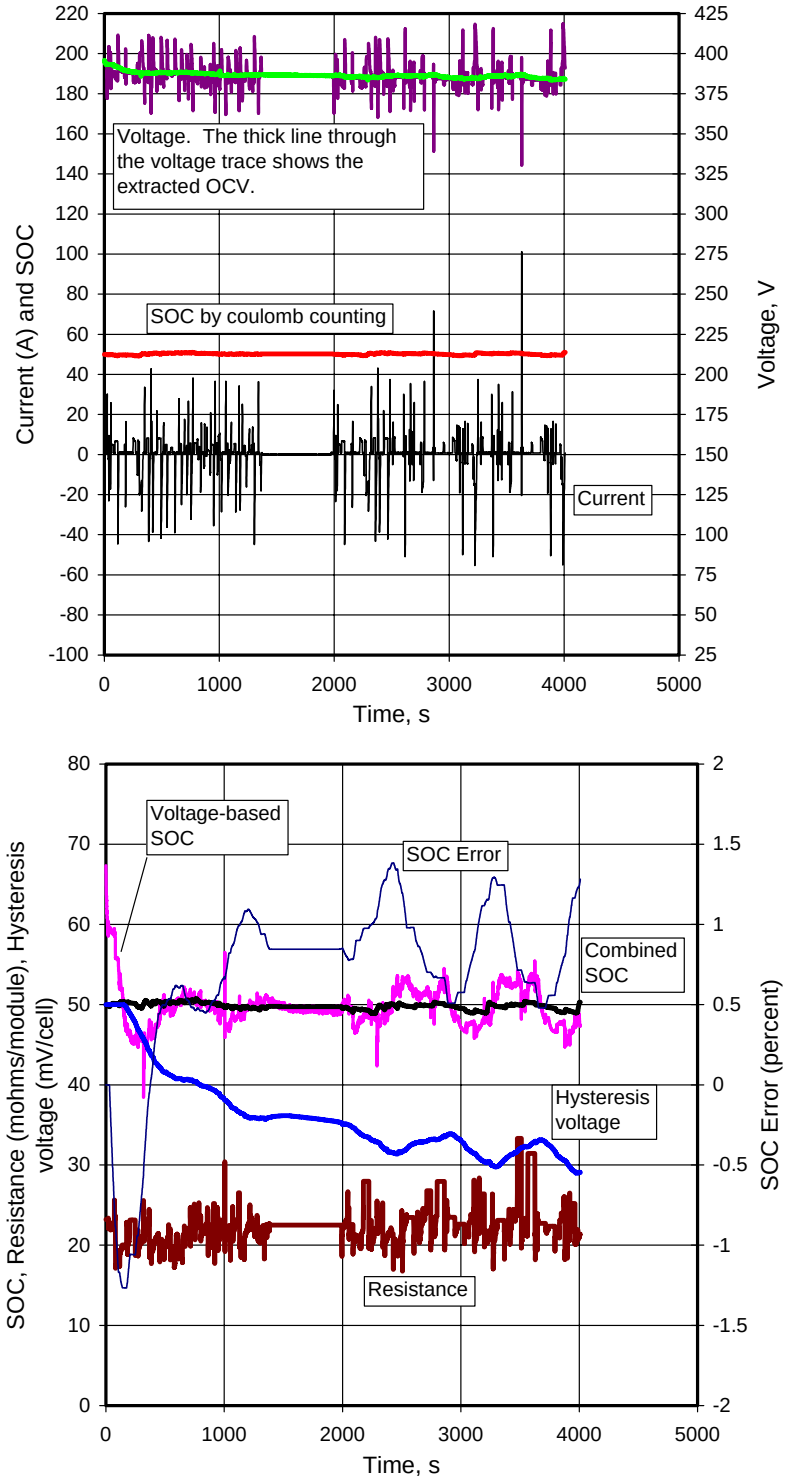


Fig. 8. Algorithm applied to data shown in Fig. 7. The voltage and current correspond to pack data; with the exception of the percent error, all other results are outputs of the algorithm.

$100(SOC_{pure\ coulomb\ counting} - SOC)/SOC_{pure\ oulomb\ counting}$. Other quantities plotted in the lower portion of Fig. 8 include the extracted module resistance (about 23 mΩ per module throughout this work, corresponding to a pack resistance of 650 mΩ as shown in Fig. 7), the regressed combined state of charge (SOC), and the regressed voltage-based state of charge ($SOC_V$). The hysteresis voltage declines from nearly 50 mV per cell initially, reflecting a battery that had just been charged, indicating that the operation of the battery system is largely charge sustaining throughout the test.

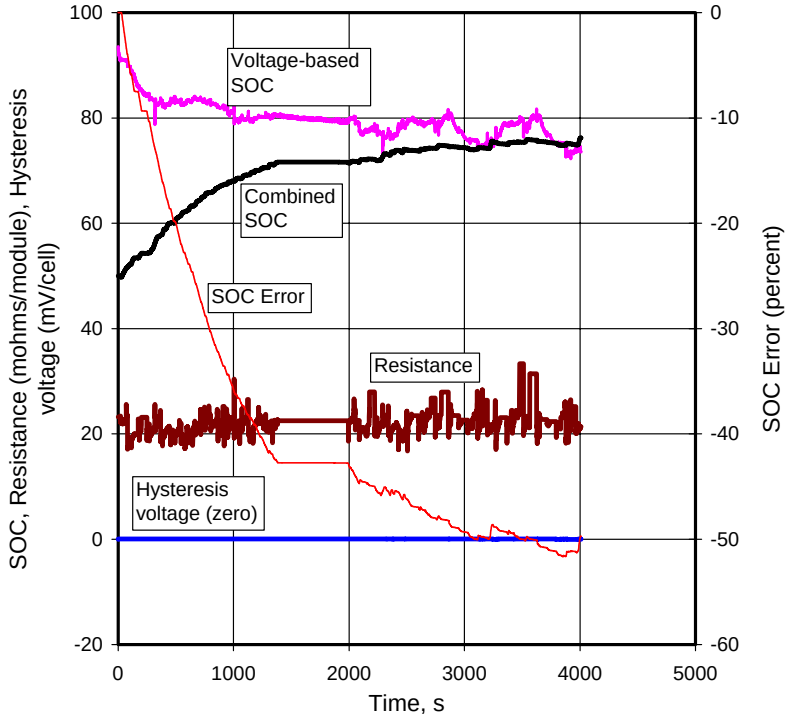


Fig. 9. Importance of hysteresis voltage. The hysteresis voltage is set to zero throughout the algorithm application; all other conditions are identical to Fig. 8. The percent SOC error is seen to be much larger that that of Fig. 8.

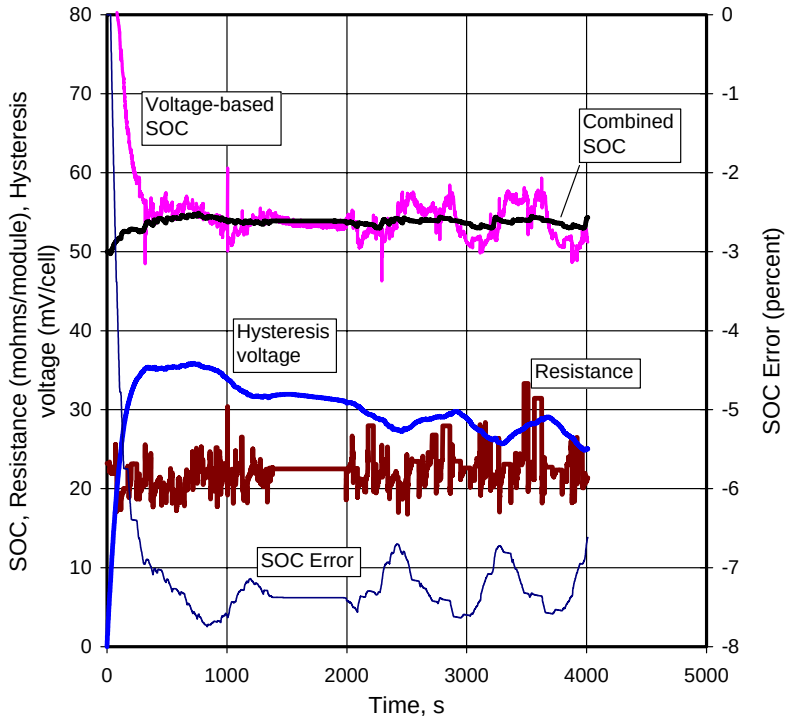


Fig. 10. Effect of initial hysteresis voltage value. Although the battery was charged immediately prior to the experiment, the hysteresis voltage initially was set to zero (cf. Fig. 8).

The importance of the hysteresis in extracting the correct SOC is made clear in Fig. 9, where $V_H$ has been set to zero. The SOC initially is correct, as it was set to the correct 50% value, but by the end of the run it is seen that error in the SOC is nearly 50%. The initial value for the hysteresis voltage is not critical, and the adaptability of the algorithm in terms of extracting $V_H$ is demonstrated in Fig. 10. We see that when the initial value for $V_H$ is set to 0 mV per cell, instead of the correct value of +50 mV per cell after charge, the algorithm tends to "converge" in a couple minutes, and the error in the SOC is never prohibitively large. This implies a rather stable algorithm.

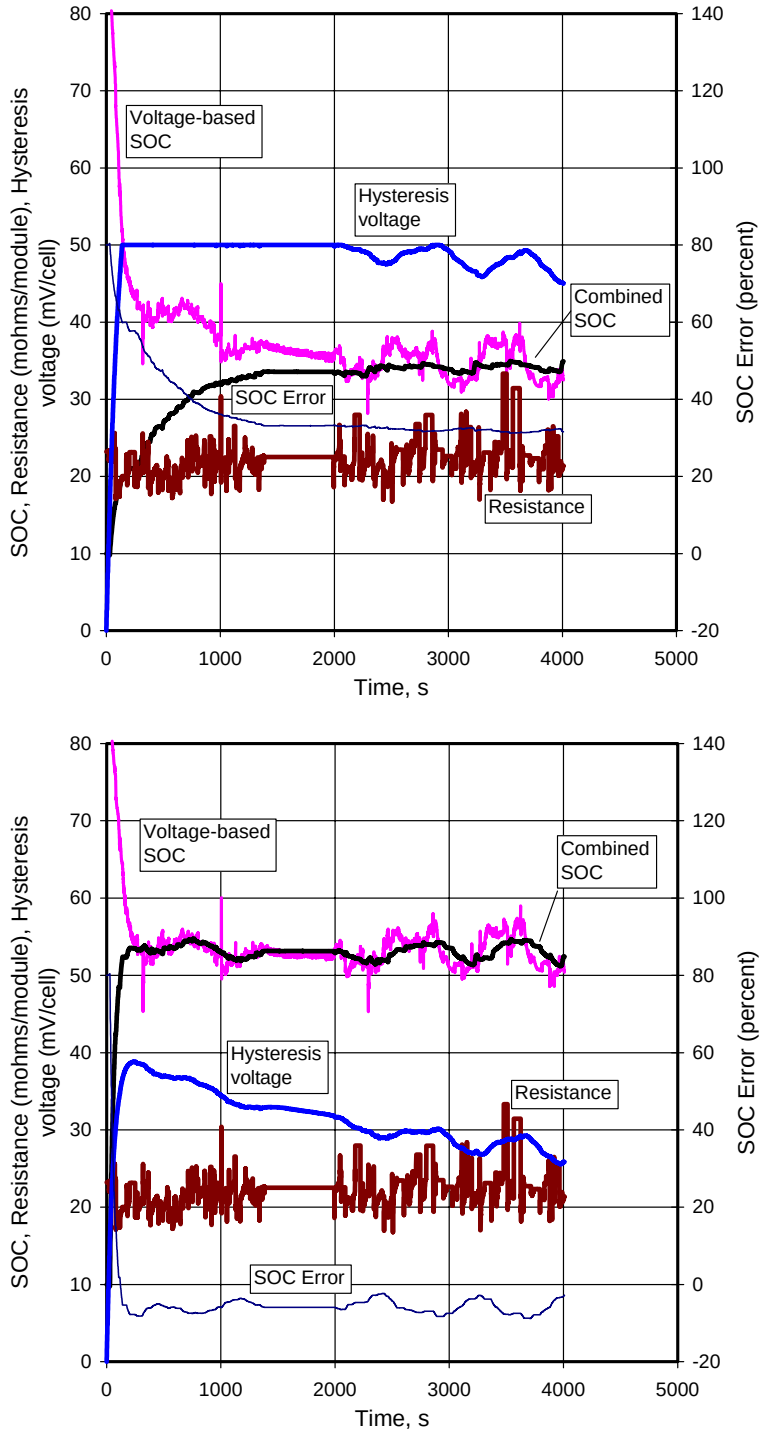


Fig. 11. Robustness test. As in the previous figure, the hysteresis voltage was set to zero initially. In addition, the beginning SOC used to start the algorithm was set to 10% (instead of the actual 50%). Upper figure: $\alpha_w = 0.001\,s^{-1}$. Lower figure: $\alpha_w = 0.01\,s^{-1}$ (more adaptive). The error in the regressed SOC is less than 10% within 100 s.

A more severe test of the algorithm rate of convergence and stability is depicted in Fig. 11, where the initial SOC for the algorithm is set to 10%, even though the actual initial SOC is 50%. By comparing the upper and lower plots, we see that in order to speed convergence of the algorithm to less than a couple minutes, the weighting of the voltage-based portion of the algorithm must be increased. The lower panel demonstrates superior convergence properties with the larger value of $\alpha_{w,50\%SOC} = 0.01\,s^{-1}$. However, the combined SOC shows more variation (albeit still acceptably stable), and an expected tradeoff between stability and adaptability must be comprehended in application. We have found it

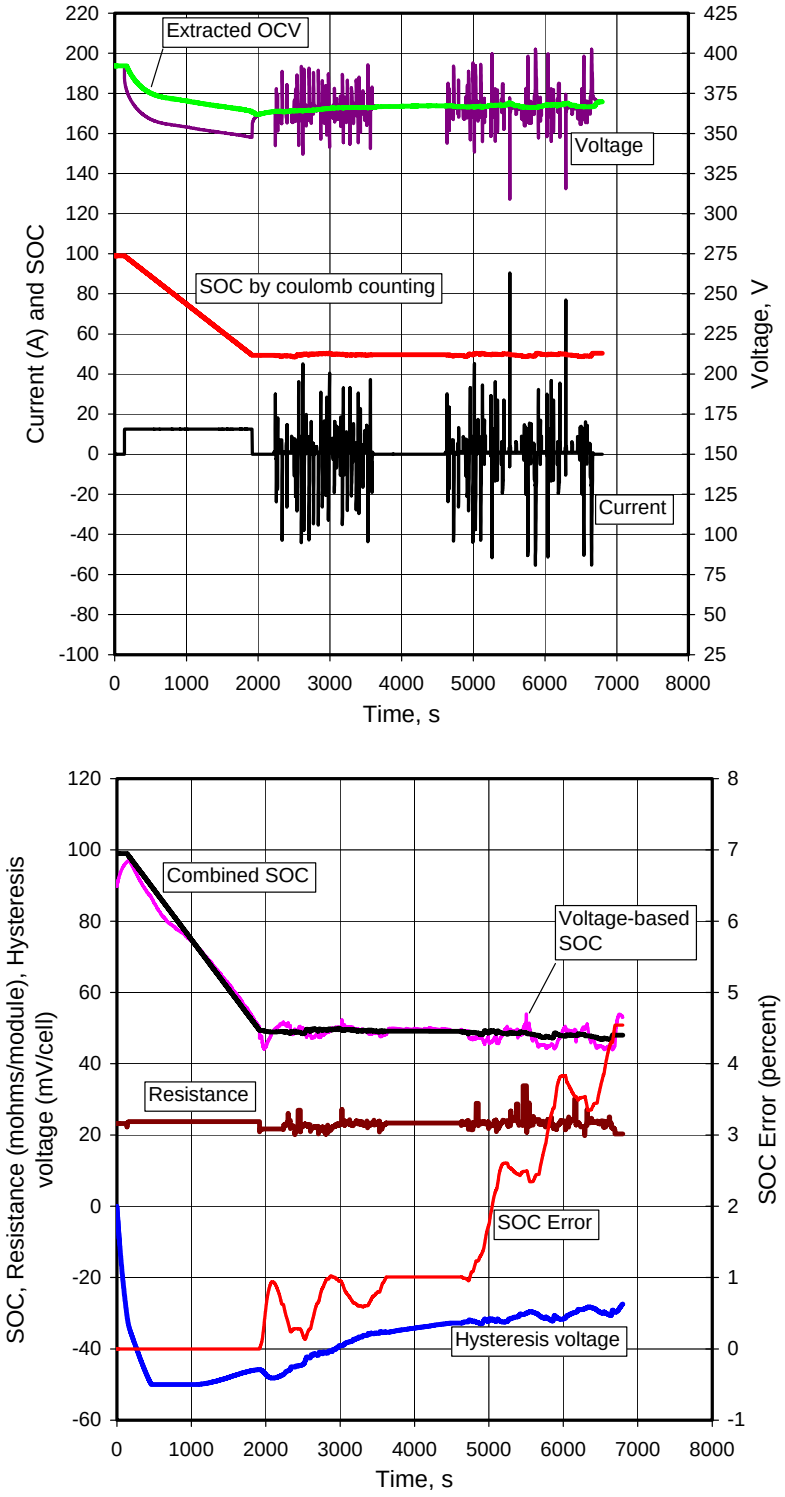


Fig. 12. Effect of prior discharge on algorithm. After the nearly 2000 s discharge, the power profile is very similar to that of Fig. 8.

useful to leave $\alpha_{w,50\%SOC}$ at $0.001\,s^{-1}$ unless a need arises to reset the algorithm (e.g., a controller reset command as might be expected in a service environment).

The effect of prior discharge on the algorithm behavior, unlike the early charge event investigated in Fig. 8, is explored in Fig. 12. After the nearly 2000 s discharge, the power profile of Fig. 12 is very similar to that of Fig. 8. In general, the results are similar to those of Fig. 8, although the error is a bit larger. Further tuning of the algorithm [4] can reduce this error (e.g., deceasing $\beta_{discharge}$ reduces the error in this case). The last investigation involves application of the algorithm to a high power profile, characteristic

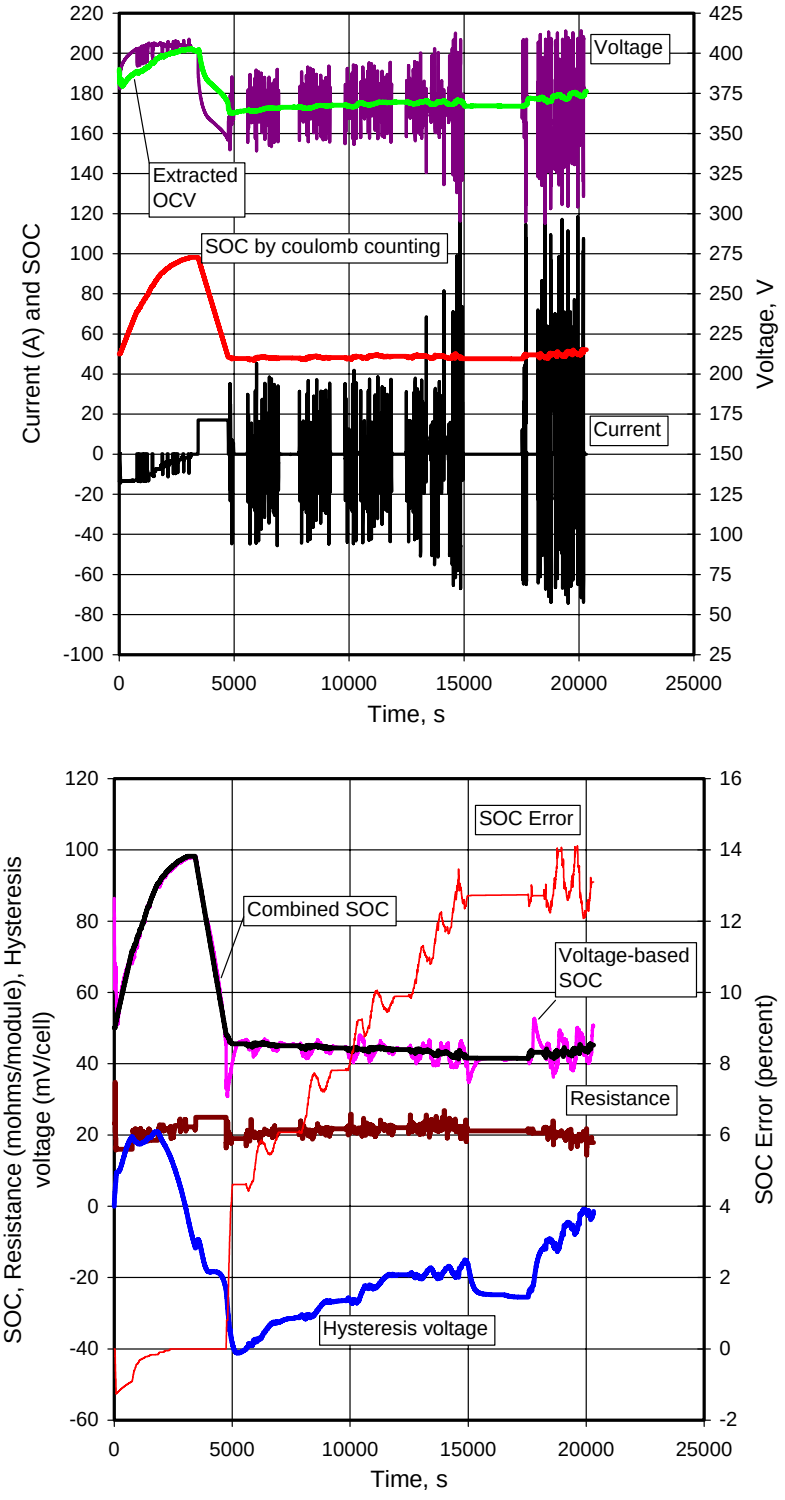


Fig. 13. Algorithm applied to high power schedule. The power after charge (i.e., after 3500 s) corresponds to a US06 schedule for the Precept.

of what the Precept sees over the aggressive US06 schedule. The magnitude of the current and voltage variations are seen to be much greater in Fig. 13 than in the earlier figures. The error in the algorithm is also larger, but the error in pure coulomb counting is also compromised at high rates of charge, and it is not unexpected that the combined SOC is less than that calculated by purely coulomb counting, as larger charge inefficiencies [27,28] are not included in the pure coulomb counting.

The previous analyses indicate that the algorithm is sufficiently accurate of the range of conditions investigated. Once the OCV and high-frequency resistance $R$ have been extracted, it is possible to estimate the charge and discharge power capability of the battery pack, which is important in terms of operating the vehicle efficiently (i.e., such knowledge is key to determining optimal torque allocation with respect to the heat engine and the electric motors). The max discharge power can be expressed as:

$$P_{\max,\text{discharge}} = IV = IV_{\min}.$$

That is, when the battery voltage obtains its lowest acceptable value, the max discharge power results. First consider an ohmic battery, wherein the superposition integral can be ignored. For the ohmic battery, $V = V_{\text{oc}} - IR$, and

$$P_{\max,\text{discharge}} = IV_{\min} = \frac{(V_{\text{oc}} - V_{\min})}{R} V_{\min}.$$

Similarly, the max charge power for the ohmic battery is given by

$$P_{\max,\text{charge}} = IV_{\max} = \frac{(V_{\text{oc}} - V_{\max})}{R} V_{\max}.$$

The ohmic battery does not address transient effects such as those correlated by the superposition integral. To improve the estimate by including transient effects, we employ Eq. (6) to determine the current:

$$I|_t = \frac{(V_{\text{oc}} - V)_t + \exp(-B\,\Delta t)[V - (V_{\text{oc}} - IR)]_{t-\Delta t}}{R + A\,\Delta t},$$

$$P_{\max,\text{discharge}} = IV_{\min} = \left[\frac{(V_{\text{oc}} - V_{\min})_t + \exp(-B\,\Delta t)[V - (V_{\text{oc}} - IR)]_{t-\Delta t}}{R + A\,\Delta t}\right] V_{\min},$$

and

$$P_{\max,\text{charge}} = IV_{\max} = \left[\frac{(V_{\text{oc}} - V_{\max})_t + \exp(-B\,\Delta t)[V - (V_{\text{oc}} - IR)]_{t-\Delta t}}{R + A\,\Delta t}\right] V_{\max}.$$

To implement these equations, the respective powers are calculated immediately after the algorithm has been employed to finish the SOC determination at time $t$. In this case, quantities calculated or measured at time $t$ are then stored in the variables listed in the respective power expressions at time $t - \Delta t$. Then one must state the duration corresponding to the desired estimate for power. It is sufficiently accurate not to update $V_{\text{oc}}$ unless $\Delta t$ were to exceed many seconds. One could then use coulomb counting on the projected current to estimate a new state of charge and update $V_{\text{oc}}$. It is ironic that while the flatness in the SOC–OCV curve gives rise to great difficulty in determining the NiMH battery SOC, it is this same lack of variation in the OCV that allows NiMH batteries to provide nearly constant charge and discharge power capability over a large range of SOC's, which is useful when it comes to constructing optimal vehicle-control algorithms.

## 5. Conclusion

Efficient vehicle operation requires the knowledge of the battery state; i.e., how much energy is left in the battery and how much power the battery discharge or accept. In addition, on-board diagnostics for the battery in a hybrid electric vehicle are required. The algorithm developed and implemented in this work represents a potential means to address these issues. Calibration changes from values employed in this work are to be expected, but the overall approach is seen to yield a substantially stable and robust algorithm over a fairly broad range of application. More testing is needed, however, to ascertain the errors in the algorithm and conditions under which the algorithm might fail to perform acceptably. Specific conclusions from this work are as follows.

1. A model-reference adaptive system based on the equivalent circuit displayed in Fig. 4 provides SOC accuracy to within ±10% for the Precept battery system over the Federal Test Procedure schedule. However, harsher drive schedules may yield less accurate results, and the measurement error employed in this work may be of the same level of error as that of the algorithm under high-power excitation.
2. NiMH batteries exhibit a large hysteresis voltage, as the voltage versus SOC curve under effectively equilibrium conditions is dependent on whether the battery is being charged or discharged (cf. Fig. 3). This effect is more pronounced at higher currents. We show that an adaptive hysteresis contribution is critical to the algorithm's successful implementation.
3. When the algorithm is started arbitrarily with an incorrect initial state (e.g., incorrect initial SOC and hysteresis voltage), about 100 s are required for convergence. In practice this arbitrary initial condition should not occur, but the result implies algorithm stability and robustness. Such behavior should facilitate service procedures on the battery pack as well.

## Acknowledgements

Many engineers and scientists at GM ATV and GM R&D contributed to this work. Shawn Sarbacker, the energy management systems engineer for the Precept, provided NiMH pack data, as did colleagues at GM Ovonics (now Texaco Ovonic Battery Systems). Valuable discussions were had with Ramona Ying, Brian Koch, Damon Frisch, Bob Conell, and Robin Vidas.

## Appendix A

*Derivation of voltage recursion relation*. In this section we derive the voltage recursion relation. We begin with the superposition integral solution of Eq. (3):

$$V = V_{\mathrm{oc}} - IR + A\int_{\zeta=t}^{\zeta=0} I(\zeta)\exp[-B(t-\zeta)]\mathrm{d}\zeta.$$

This expression is based on the assumption that $I(t) = 0$ for $t < 0$. At time zero,

$$(V - V_{\mathrm{oc}} + IR)_{t=0} = 0.$$

For the first time step,

$$(V - V_{\mathrm{oc}} + IR)_{t=t_1} \approx -\mathrm{e}^{-Bt_1}A(I_{t=t_1})\mathrm{e}^{Bt_1}\,\Delta t_1,$$

or

$$(V - V_{\mathrm{oc}} + IR)_{t=t_1}\mathrm{e}^{Bt_1} \approx -A(I_{t=t_1})\mathrm{e}^{Bt_1}\,\Delta t_1,$$

where the current in the integrand has been taken constant over the time step. For the second time step,

$$(V - V_{\mathrm{oc}} + IR)_{t=t_2} \approx \mathrm{e}^{-Bt_2}\left[-A(I_{t=t_2})\mathrm{e}^{Bt_2}\,\Delta t_2 - A(I_{t=t_1})\mathrm{e}^{Bt_1}\,\Delta t_1\right],$$

or

$$(V - V_{\mathrm{oc}} + IR)_{t=t_2} \approx -A(I_{t=t_2})\Delta t_2 + \mathrm{e}^{-B\,\Delta t_2}(V - V_{\mathrm{oc}} + IR)_{t=t_1}.$$

Following this procedure, similar recursion relations result for subsequent time steps, with the general expression corresponding to

$$V_t = (V_{\mathrm{oc}} - IR)_t - A(I_t)\Delta t + \mathrm{e}^{-B\,\Delta t}(V - V_{\mathrm{oc}} + IR)_{t-\Delta t}.$$

This corresponds to Eq. (6). The utility of the recursion relation stems from the fact that time integration of past currents need not be used to determine the voltage; only the present and previous time-step values are required. It should be recognized that there are other methods to approximate the integral that are equivalent from an implementation point of view when it comes to constructing a recursive voltage-current relation for SOC and SOH extraction. For example, one can average the current over the time step, giving rise to the factor $(I_{t-\Delta t} + I_t)/2$ multiplying on to $A$. Higher-order approximations could be employed. Since the expression is placed in an adaptive routine, and the time steps in practice are to be taken as small relative the characteristic time $1/B$, effectively identical results are obtained with higher-order approximations.

## References

[1] M. Verbrugge, E. Tate, S. Sarbacker, B. Koch, Quasi-Adaptive State of Charge Algorithm of Nickel-Metal Hydride Batteries, United States Patent 6359419, 19 March 2002.
[2] E. Meissner, G. Richter, J. Power Sources 116 (2003) 79–98.
[3] A. Gelb (Ed.), Applied Optimal Estimation, MIT Press, Cambridge, MA, 1974.
[4] P.S. Maybeck, Stochastic models, estimation and control, in: Mathematics in Science and Engineering, vol. 141-1, Academic Press, 1979.
[5] B. Widrow, S.D. Stearns, Adaptive Signal Processing, Prentice-Hall, Englewood Cliffs, NJ, 1985.
[6] L. Ljnug, T. Söderström, Theory and Practice of Recursive Identification, MIT Press, Cambridge, MA, 1986.
[7] K.J. Åström, B. Wittenmark, Adaptive Control, Addison-Wesley, Reading, MA, 1989.
[8] L. Ljnug, System Identification: Theory for the User, Prentice-Hall, Englewood Cliffs, NJ, 1987.
[9] R. Kulhavý, Recursive Nonlinear Estimation. A Geometric Approach, Springer, London, 1996.
[10] D. Fan, R. White, J. Electrochem. Soc. 138 (17) (1991) 2952.
[11] B. Paxton, J. Newman, J. Electrochem. Soc. 144 (1997) 3818.
[12] O. Barbarisi, R. Canaletti, L. Glielmo, M. Gosso, F. Vasca, in: Proceedings of the 41st IEEE Conference on Decision and Control, Las Vegas, NV, December 2002.
[13] P. Milner, U. Thomas, in: C.W. Tobias (Ed.), Advanceds in Electrochemistry and Electrochemical Engineering, Interscience Publishers, New York, NY, 1967.
[14] X.G. Yang, B.Y. Liaw, J. Electrochem. Soc. 148 (2001) A1023.
[15] K.P. Ta, J. Newman, J. Electrochem. Soc. 146 (1999) 2769.
[16] W.B. Gu, C.Y. Wang, J. Electrochem. Soc. 147 (2000) 2910.
[17] V. Srinivasan, J.W. Weidner, J. Newman, J. Electrochem. Soc. 148 (2001) A969.
[18] M.W. Verbrugge, Proceedings Volume from the 17th International Electric Vehicle Symposium, Montreal, Canada, October 2000.
[19] M.W. Verbrugge, R.S. Conell, Proceedings Volume from the 18th International Electric Vehicle Symposium, Berlin, Germany, October 2001.
[20] M.W. Verbrugge, R.S. Conell, J. Electrochem. Soc. 149 (2002) A45.
[21] P. Delahay, Double Layer and Electrode Kinetics, Interscience Publishers, New York, NY, 1965.
[22] D.D. Macdonald, Transient Techniques in Electrochemistry, Plenum Press, New York, NY, 1977.
[23] A.J. Bard, L.R. Faulkner, Electrochemical Methods. Fundamentals and Applications, Wiley, New York, NY, 1980.
[24] J.W. Weidner, P. Timmermann, J. Electrochem. Soc. 141 (1994) 349.
[25] R.M. Felder, R.W. Rousseau, Elementary Principles of Chemical Processes, Wiley, New York, NY, 1978, pp. 501–503.
[26] W.H. Beyer (Ed.), Standard Mathematical Tables, 24th ed., CRC Press, Cleveland, OH, 1976, pp. 476–477.
[27] Z. Zhang, M. Zhong, F. Liu, F. Zhong, F. Wu, J. Power Sources 70 (1998) 276.
[28] D.-M. Kim, H. Lee, K.-J. Jang, J.-Y. Lee, J. Electrochem. Soc. 145 (1998) 3387.